Functional Materials Letters
Vol. 10, No. 6 (2017) 1750081 (5 pages)

DOI: 10.1142/S1793604717500813

World Scientific
www.worldscientific.com

Superconcentrated aqueous electrolyte to enhance energy density for advanced supercapacitors

Zengying Tian*, Wenjun Deng*, Xusheng Wang†, Chunyi Liu*, Chang Li*, Jitao Chen†, Mianqi Xue*,‡, Rui Li*,¶ and Feng Pan*,‖

*School of Advanced Materials, Shenzhen Graduate School
Peking University, Shenzhen 518055, P. R. China

†Beijing National Laboratory for Molecular Sciences
College of Chemistry and Molecular Engineering
Peking University, Beijing 100871, P. R. China

‡Institute of Physics and Beijing National Laboratory
for Condensed Matter Physics
Chinese Academy of Sciences
Beijing 100190, P. R. China
¶lirui@pkusz.edu.cn
‖panfeng@pkusz.edu.cn

Received 22 September 2017; Accepted 30 October 2017; Published 22 November 2017

We here report a superconcentrated potassium acetate (KAC) solution (75 wt.%, K : H_2O = 1 : 1.8, called as "water-in-salt") as an aqueous electrolyte to improve the working voltage and increasing capacitance in enhancing the energy density of the active carbon-based aqueous supercapacitor. The stability potential window of the superconcentrated electrolyte realizes an AC//AC symmetric supercapacitor with operating voltage of 2.0 V and excellent cyclic performance. Meanwhile, the energy density of such supercapacitor achieves about twice as high as that of the supercapacitor using normal concentration of electrolyte.

Keywords: Superconcentrated aqueous electrolyte; potassium acetate; high voltage; symmetric supercapacitors.

Supercapacitors have attracted considerable interest due to their fast charge/discharge processes (within a few seconds) and long cycle life (over 100,000 times).[1] So far, different materials, such as graphene and numerous two-dimensional (2D) materials,[1–7] conducting polymers,[2,8] metal oxides,[9–11] carbon/carbides and their composites,[12–14] have been tried to fabricate high-performance supercapacitors. Meanwhile, direct laser writing,[15] three dimensional (3D) printing,[16] soft lithography,[17–19] direct pen writing,[20–22] in-situ polymerization,[23–25] electrospinning,[26–28] and many other advanced technologies[29] have been developed constantly to improve the energy storage performances,[30,31] flexibility,[32] integration level,[32,34] microminiaturization,[35] light permeability,[36] and even intelligence of supercapacitors.[37,38] However, the major issue of poor energy density limits their applications. Taking the following formula into consideration:

$$E = 0.5CU^2, \quad (1)$$

where C represents the capacitance, U is the operating cell voltage, and E is the energy released by a supercapacitor. Note that increasing the operating voltage would be more efficient than increasing the capacitance in terms of the improvement of energy density, and the operating cell voltage of supercapacitors mainly depends on the electrochemical stability window of the electrolytes. Hence, developing novel electrolytes with wide potential windows is very necessary.

Aqueous electrolytes present obvious advantages compared with organic electrolytes, such as low cost, high safety, environmental friendliness, high conductivity and manageability.[39–42] Yet their main disadvantage is the relatively narrow potential window, which is induced by the decomposition of water. The operating voltages of these aqueous supercapacitors usually can only reach 1.23 V arising from the O_2 and H_2 evolution. In order to solve the problem, Suo *et al.*[40] recently reported the superconcentrated salt solution (called as "water-in-salt" electrolyte) which provided

¶Corresponding author.

an expanded electrochemical stability window of ∼ 3.0 V. The water activity is reduced as a result of the super-concentrated salt solution as well as an inner Helmholtz layer, which helps to inhibit the O_2 evolution on the cathode side.[41] Yamada and coworkers[42] reported the employment of a hydrate-melt Li salt electrolyte to broaden the voltage window of aqueous batteries. For the hydrate melt, the anodic limit is expanded to 5.05 V and the cathodic limit is extended down to 1.25 V (versus Li/Li^+). Hasegawa *et al.* reported the practical symmetric AC//AC (active carbon, AC) super-capacitor involving "water-in-salt" electrolyte (5 M LiTFSI) allowed a maximum operating voltage of 2.4 V with good cyclic performance.[43] Here, we report the first utilization of the superconcentrated potassium acetate (KAC) solution as high-voltage aqueous electrolyte and the AC as active materials of electrodes in fabricating AC//AC symmetric supercapacitors. The superconcentrated (75 wt.%, K : H_2O = 1 : 1.8) KAC aqueous electrolyte possesses an expanded stability potential window of ∼ 2.5 V, and this system exhibits an operating voltage of 2.0 V with 88% capacitance retention after 10,000 cycles.

The electrochemical stability windows of different solutions were measured on a platinum electrode via cyclic voltammetry (CV). The electrochemical stability window expands greatly with the increase of the KAC concentration, while both oxygen and hydrogen evolution voltages are pushed beyond the thermodynamic stability limits of water. As shown in Fig. 1(a), the onset hydrogen evolution voltage is −1.25 V (versus SCE, saturated calomel electrode) for K-75 solution. This passivation eventually suppresses hydrogen evolution from −0.9 V to −1.25 V. Similarly, the cathodic polarization current decreases sharply as the concentration of the KAC increases. Meanwhile, oxygen evolution also seems to be suppressed on the cathode side due to the reduced water activity as well as an inner Helmholtz layer. When the coordinated K^+ is at high concentration, the highest occupied molecular orbital (HOMO) level is lowered due to the donation of electrons of the H_2O molecules from the lone pair of the oxygen atom.[44] As a result, its oxidation potential is raised. Overall, the highest stability window of ∼ 2.5 V is achieved in the K-75 solution with both the anodic (1.25 V versus SCE) and cathodic (−1.25 V versus SCE) improvements, while the stability window is only 1.9 V for the K-10 solution (Fig. 1(b)). The preparation of the K-75 solution is shown in Fig. 1(c). Around 25% of water was dissolved in 75% KAC salt. After dissolving completely, the volume of the solution becomes large and its molality is 7.64 mol/kg.

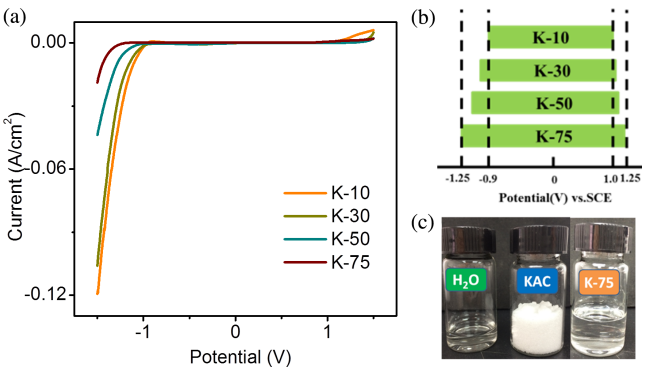

Fig. 1. (a) The electrochemical stability window of KAC electrolytes, which were measured between −1.5 V and 1.5 V versus SCE at 10 mV/s, using platinum as working and counter electrodes. (b) Relationship between the potential windows and the four different concentrations of KAC solution. (c) 25 wt.% water and 75 wt.% KAC used to prepare a superconcentrated KAC solution (K-75).

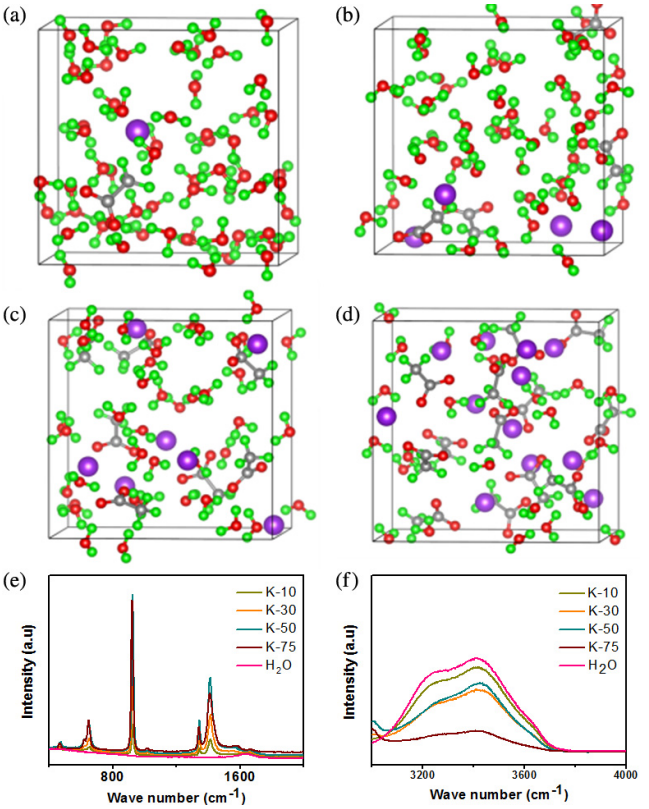

Fig. 2. Illuminations of (a) K-10, (b) K-30, (c) K-50 and (d) K-75 solutions, which were obtained from first-principles DFT-MD simulation. Atom colors: K = purple; O = red; C = gray; H = green. (e) Raman spectra of the four different concentration solutions of KAC. (f) Magnified view of the range between 3000–4000 cm^{-1} in panel (e). The Raman bonds observed in the range of 3000–3800 cm^{-1} correspond to the O–H stretching modes of water molecules.

The conductivities and pH values of the electrolytes with different concentrations are shown in Table S1. To gain theoretical insight into the liquid structures, we performed first-principles DFT-MD simulations. In K-10 and K-30 solutions, K^+ is solvated by water molecules, and many free water molecules form a network with each other through hydrogen bonding (Figs. 2(a) and 2(b), respectively). The structure of K-50 solution in Fig. 2(c) exhibits the decreased

free water molecules. In the K-75 solution (Fig. 2(d)), most of the water molecules are coordinated with K^+ by the Lewis-basic oxygen atoms and form "water-in-salt" molecules.[42] The Raman spectrum shows the O–H stretching vibration of water molecules in different solutions (Figs. 2(e) and 2(f)). In pure water, the broad Raman band (3000–4000 cm^{-1}), caused by the O–H stretching vibration corresponds to various water molecules with different hydrogen-bonding environments in water clusters. The intensity of the broad Raman band decreases obviously with the increase of the concentration of KAC salt, indicating the diminished abundance of water clusters and the formation of "water-in-salt" molecules. This result is consistent with the above-mentioned simulations.

A higher potential window would bring a higher operating voltage for supercapacitors. To confirm the assumption, CVs of symmetric AC//AC two-electrode capacitors at an extended voltage were applied using different concentrations of KAC electrolyte (as shown in Fig. 3). A significant increase of anodic current can be observed as the scanning voltage increases from 1.6 to 2.0 V, especially for the supercapacitor with K-10 electrolyte. The high polarization current suggests a more serious decomposition of electrolyte, and the polarization current decreases as the concentration of KAC electrolyte increases, (Fig. S1). Figure 3(d) reveals a very little change of anodic current as the scanning voltage shifting to 2.0 V for K-75, the CV curves are characteristic of approximate rectangle, which means that the symmetric supercapacitor presents a double-layer storage without decomposition of the electrolyte. It should be noted that the performances of the superconcentrated electrolyte in the pseudocapacitance system (such as conducting polymers, metal oxides and chalcogenides)[8–11,45–47] need to conduct further research.

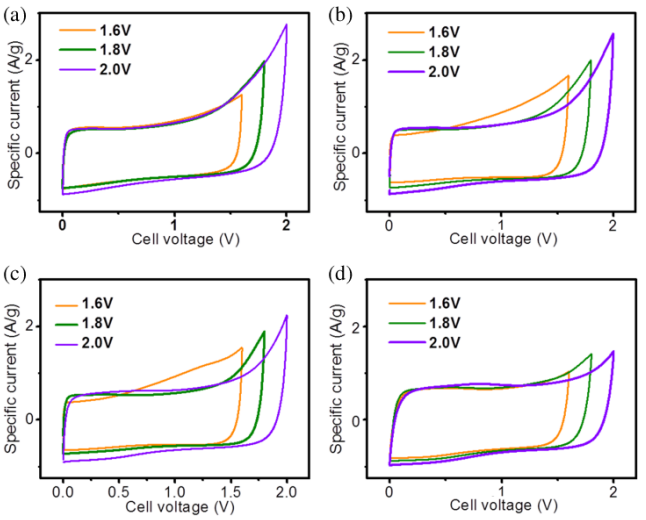

Fig. 3. Comparison of the CV profiles performed in a two-electrode AC// AC supercapacitor at 10 mv s^{-1} in different concentrations of KAC electrolytes with stepwise shifting of the voltage of 0.2 V. (a) K-10 electrolyte, (b) K-30 electrolyte, (c) K-50 electrolyte, (d) K-75 electrolyte.

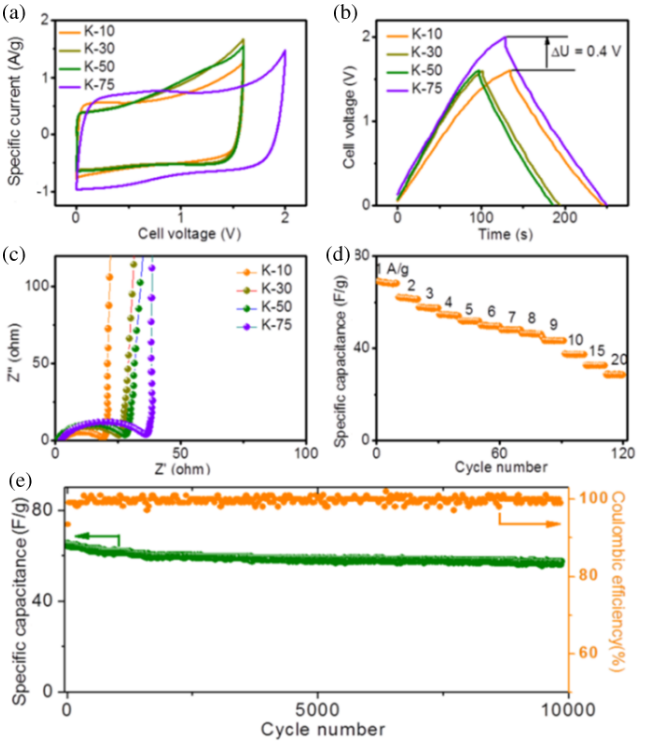

Fig. 4. (a) CVs (10 mv s^{-1}) of the two-electrode AC//AC capacitors using the four KAC electrolytes up to different voltages. (b) Corresponding charge and discharge curves at 1 A g^{-1}. (c) Nyquist spectra of the two-electrode capacitors in different aqueous electrolytes in the frequency range from 100 kHz to 10 mHz. (d) Rate performance of the supercapacitors in the K-75 electrolyte with the current density from 1 to 20 A g^{-1}. (e) Cycling stability of the AC//AC supercapacitor with 2.0 V at the current density of 1 A g^{-1}.

The CV results demonstrate that superconcentrated electrolyte (K-75) enables an operating voltage of 2.0 V, while the operating voltage for other low-concentration electrolytes is below 1.6 V to avoid the decomposition of water (as shown in Fig. 4(a)). When the operating voltage rises to 2.0 V, the charge/discharge curves causes deformation due to the evolution of oxygen (Fig. S2). Figure 4(b) shows the galvanostatic charge/discharge curves for the different electrolytes. The curves with symmetrical triangular shape demonstrate a pure capacitive behavior and excellent coulombic efficiency. By using K-75 electrolyte, the working voltage have increased by 0.4 V compared with using low-concentration electrolytes, which will enhance the energy density a lot due to E versus U^2 in Eq. (1). The Nyquist impedance spectra of the two-electrode supercapacitors with different aqueous electrolytes in Fig. 4(c) present a typical capacitive shape. At high frequencies (100 kHz), the resistance is mainly dominated by an electrolyte resistance, and the real part impedance Re(Z') with K-30 electrolyte is smallest, which reflects the highest conductivity (116.4 mS/cm for K-30, see in Table S1). But in general, they are very close, indicating a negligible effect on the resistance at high frequency region. The semicircle in the middle frequency range is larger in

K-75 than in all the other electrolytes, which is correlated with the electrolyte resistance within pores and contact resistance. The contact resistance should be the same in the two-electrode capacitor, therefore the difference in arc portion is dependent on the electrolyte resistance within pores, which is closely related to the different conductivities and viscosities of the electrolytes. Along with the increase of molality, the viscosity of the electrolyte increases, suggesting that the ion diffusion slows down and eventually leads to a large internal resistance.

Besides the expanded operating voltage, it was found that the concentrated electrolyte also leads to the capacitance increase of the supercapacitors. The symmetric AC//AC supercapacitor with K-75 electrolyte shows the highest capacitance (twice of the capacitances with lower–concentrated electrolytes, Table S2). The CV curves of the monolithic electrode in three-electrode cells also demonstrate the increase in capacitance with the electrolytes (Fig. S3). The increase in capacitance is probably due to the decrease of the radius of hydrated K^+ and $CH3COO^-$. The superconcentrated electrolyte (K-75) corresponds to a stoichiometric compound $KAC(H_2O)_{1.82}$. Apparently, the radius of the $K(H_2O)^+_{1.82}$ is smaller than that of the full hydrated K^+ ($K(H_2O)^+_7$ ~2.80 Å).[48] Feng *et al.* had developed a sandwich capacitance model to predict the anomalous enhancement of capacitance that has been experimentally verified in micropores.[49] The smaller hydrated ions are more likely to enter the micropores, leading to a higher capacitance.[50,51] Figure 4(d) shows the rate performance of the AC//AC supercapacitor using K-75 electrolyte under various current densities. K-75 electrolyte displays a roughly equivalent rate performance with other three electrolytes (Fig. S4). At a low current density of 0.5 A/g, a high capacitance of 69 F/g is presented. The capacitance values are 37.4, 32.7 and 28.6 F/g, corresponding to the current densities at 10, 15 and 20 A/g, respectively. Figure 4(e) shows the cycling stability of capacitors in the K-75 electrolyte at the current density of 1 A/g. After 10,000 cycles, the capacitance value of the supercapacitor decreases a little bit (with high capacitance retention of 88% from 65 to 57 F/g). Self-discharge performance is a main gauge of supercapacitors, the one with superconcentrated K-75 electrolyte also exhibits a lower self-discharge rate (Fig. S5). The Ragone plot of AC//AC supercapacitors with different concentrations of KAC electrolytes is shown in Fig. S6. The energy density can reach 19.8 Wh/kg at a power density of 500 W/kg, and still remains 9.6 Wh/kg at a power density of 20 kW/kg, suggesting that the superconcentrated electrolyte is quite a promising candidate for aqueous supercapacitors.

In summary, we explored a superconcentrated KAC aqueous electrolyte (K-75) for symmetric AC//AC supercapacitors. Both the Raman spectra and simulation results demonstrate the formation of "water-in-salt" molecules in the K-75 electrolyte. The electrochemical stability potential window of the K-75 electrolyte is as high as 2.5 V. This superconcentrated electrolyte enables a high operating voltage (2.0 V) and an enhanced capacitance for the symmetric supercapacitor. Specifically, the energy density expands to 16.8 Wh/kg, twice of that in the supercapacitor using normal-concentration electrolyte. Meanwhile, the supercapacitor with the K-75 electrolyte delivers high capacitance retention of 88% at a high operating voltage of 2.0 V over 10,000 cycles. Therefore, the success utilization of the superconcentrated KAC electrolyte in fabricating supercapacitor provides a new direction in exploiting the high performance aqueous supercapacitors.

Acknowledgments

This work was supported by the Shenzhen Science and Technology Research Grant (JCYJ20160531141109132, JCYJ20170412150450297) and Guangdong Innovative and Entrepreneurial Research Team Progress (2013N080).

References

1. C. Zhong *et al.*, *Chem. Soc. Rev.* **44**, 7484 (2015).
2. M. Xue *et al.*, *Adv. Funct. Mater.* **22**, 1284 (2012).
3. P. Simon *et al.*, *Science* **343**, 1210 (2014).
4. F. W. Li *et al.*, *Adv. Funct. Mater.* **25**, 4601 (2015).
5. Y. W. Zhu *et al.*, *Science* **332**, 1537 (2011).
6. M. D. Stoller *et al.*, *Nano Lett.* **8**, 3498 (2008).
7. E. G. D. Firmiano *et al.*, *Adv. Energy Mater.* **4**, 175 (2014).
8. G. A. Snook *et al.*, *J. Power Sources* **196**, 1 (2011).
9. M. Xue *et al.*, *Nanoscale* **3**, 2703 (2011).
10. X. L. Ma *et al.*, *Nanoscale* **7**, 8715 (2015).
11. X. Y. Lang *et al.*, *Nat. Nanotechnol.* **6**, 232 (2011).
12. M. Xue *et al.*, *J. Mater. Chem. A* **3**, 7715 (2015).
13. L. L. Zhang *et al.*, *Chem. Soc. Rev.* **38**, 2520 (2009).
14. M. Arulepp *et al.*, *J. Power Sources* **162**, 1460 (2006).
15. W. Gao *et al.*, *Nat. Nanotechnol.* **6**, 496 (2011).
16. C. Zhao *et al.*, *Electrochem. Commun.* **41**, 20 (2014).
17. Z. N. Yu *et al.*, *Adv. Mater.* **25**, 3302 (2013).
18. F. F. Wang *et al.*, *Adv. Mater.* **21**, 2211 (2009).
19. M. Xue *et al.*, *Nanoscale* **4**, 1939 (2012).
20. Q. Jiang *et al.*, *Adv. Funct. Mater.* **25**, 4976 (2015).
21. M. Xue *et al.*, *Adv. Mater.* **27**, 3614 (2015).
22. Y. Z. Zhang *et al.*, *Chem. Soc. Rev.* **44**, 5181 (2015).
23. M. Xue *et al.*, *Adv. Mater.* **28**, 8265 (2016).
24. M. Xue *et al.*, *Adv. Mater.* **27**, 5923 (2015).
25. G. F. Ma *et al.*, *J. Power Sources* **229**, 72 (2013).
26. C. Kim *et al.*, *Appl. Phys. Lett.* **83**, 1216 (2003).
27. M. Xue *et al.*, *Nanoscale* **5**, 1803 (2013).
28. Z. Zeng *et al.*, *J. Power Sources* **358**, 22 (2017).
29. C. W. Shen *et al.*, *Sci. Rep.* **3**, 2294 (2013).
30. M. Acerce *et al.*, *Nat. Nanotechnol.* **10**, 313 (2015).
31. Z. N. Yu *et al.*, *Energy Environ. Sci.* **8**, 702 (2015).
32. Y. L. Shao *et al.*, *Chem. Soc. Rev.* **44**, 3639 (2015).
33. P. C. Du *et al.*, *Adv. Funct. Mater.* **25**, 2420 (2015).

34. Y. Huang *et al.*, *Small* **12**, 3393 (2016).
35. J. Ren *et al.*, *Adv. Mater.* **25**, 1155 (2013).
36. R. Yuksel *et al.*, *ACS Appl. Mater. Interfaces* **6**, 15434 (2014).
37. P. H. Yang *et al.*, *Angew. Chem., Int. Ed.* **53**, 11935 (2014).
38. Z. Xie *et al.*, *Chem. Commun.* **50**, 608 (2014).
39. M. Galinski *et al.*, *Electrochim. Acta* **51**, 5567 (2006).
40. L. M. Suo *et al.*, *Science* **350**, 938 (2015).
41. Y. B. Sun *et al.*, *Energy Technol.* **2**, 698 (2014).
42. Y. Yamada *et al.*, *Nat. Energy* **1**, 16129 (2016).
43. G. Hasegawa *et al.*, *Chem. Mater.* **28**, 3944 (2016).
44. J. Yu *et al.*, *Adv. Mater. Interfaces* 1700279 (2017).
45. Z. Yang *et al.*, *ACS Nano* **10**, 755 (2016).
46. X. Wang *et al.*, *Adv. Mater.* **28**, 8645 (2016).
47. M. Xue *et al.*, *Chem. Asian J.* **5**, 2266 (2010).
48. S. Varma *et al.*, *Biophys. Chem.* **124**, 192 (2006).
49. G. Feng *et al.*, *ACS Nano* **4**, 2382 (2010).
50. J. P. Randin *et al.*, *J. Electroanal. Chem.* **36**, 257 (1972).
51. M. Sevilla *et al.*, *Electrochim. Acta* **52**, 3207 (2007).